# Eigenvalue Statistics and Spatial Characteristics in Hotspot Areas Based on Wideband MIMO Channel Measurements

Xinying Gao, Jianhua Zhang, *Member, IEEE*, Yu Zhang
Key Laboratory of Universal Wireless Communications, Ministry of Education
Beijing University of Posts and Telecommunications, Beijing, China
Email: xinyinggao@gmail.com

***Abstract*—Wideband channel measurements have been performed at 5.25 GHz in hotspot areas in Beijing with a multiple-input multiple-output (MIMO) channel sounder. Based on the measured data in the indoor line-of-sight (LOS) and outdoor LOS/obstructed-line-of-sight (OLOS) scenarios, the frequency-dependent eigenvalues and average eigenvalue statistics are presented in this paper. In the indoor scenario, the probability density functions (pdfs) of the maximum and minimum eigenvalues are well fitted using the normal distribution. In the outdoor scenario, the log-normal distribution is proposed to model the pdfs of these two eigenvalues. As the indicator of spatial selectivity, the empirical cumulative distribution functions (cdfs) of condition number are obtained in two scenarios, indicating that the spatial multiplexing technique is more suitable in indoor LOS scenario than in the outdoor LOS/OLOS scenario. Additionally, the three-dimensional (3D) directional spread is calculated to illustrate the spatial dispersion of the multipath components. These information are of significance for the design and performance evaluation of MIMO communication systems employed in hotspot areas.**

## I. Introduction

With the increasing demand of high-data-rate communication services in IMT-Advanced system, multi-input multi-output (MIMO) technique coupled with high carrier frequency and wide bandwidth are suitable for the wireless applications in hotspot areas. In this scenario, both the transmitter (Tx) and receiver (Rx) are surrounded by a number of objects, resulting in the rich local scattering. In an effort to get better understanding of channel characteristics and thereby eventually design the optimal MIMO techniques, we conducted wideband MIMO channel measurements in hotspot areas in Beijing, China. The center carrier frequency is 5.25 GHz, and the bandwidth is 100 MHz.

In order to exploit the benefits of MIMO channel matrix $\mathbf{H}$, it is vital to investigate the statistical behavior of the eigenvalues of $\mathbf{H}\mathbf{H}^{\dagger}$, which play a central part in the design and analysis of MIMO systems, such as beamforming [1], spatial multiplexing [2], and space-time coding [3]. The superscript $^{\dagger}$ means Hermitian transpose. Unfortunately, to derive the distribution of eigenvalues is not an easy work. In [4], [5], expressions exist assuming all coefficients of $\mathbf{H}$ are independent and identically distributed (i.i.d.) Gaussian variables, but they are in many cases too complicated for practical use. In [6], [7], the asymptotic distribution of eigenvalues is studied under correlated fading assuming the number of antennas is large. Based on measured channel data, the eigenvalue analysis is reported in [8], [9], but without any discussion about distribution or spatial property. In contrast, we present some new results in this paper. Based on the measured MIMO channel impulse responses (CIRs) in hotspot areas, eigenvalues and spatial characteristics are investigated, including the frequency-dependent eigenvalues, distribution of the maximum and minimum eigenvalues, empirical results of condition number as well as the three-dimensional (3D) directional spread.

The rest of the paper is organized as follows. In section II, wideband MIMO channel model is given for the following analysis. The measurement system and the environment are described in Section III. Measured results and discussion are presented in Section IV. Finally, conclusions are drawn in Section V.

The research is funded by National 863 High Technology Research and Development Program of China (No. 2006AA01Z258), China Mobile Research Institute and '111' program.

## II. Wideband MIMO Channel Model

Assume $M$ antenna elements in Tx array are located at $r_{1,1}, \cdots, r_{1,M} \in \mathbb{R}^3$ with respect to a reference point $O_1$. $N$ antenna elements in Rx array are located at $r_{2,1}, \cdots, r_{2,N} \in \mathbb{R}^3$ with respect to a reference point $O_2$ [10]. The direction $\Omega$ is uniquely determined by the spherical coordinates $(\phi, \theta) \in [-\pi, \pi) \times [-\pi/2, \pi/2]$ according to

$$\Omega = [\cos(\phi)\cos(\theta), \sin(\phi)\cos(\theta), \sin(\theta)]^T, \qquad (1)$$

where $[\cdot]^T$ denotes the transpose. The angles $\phi$ and $\theta$ are referred to as the azimuth and the elevation of $\Omega$.

Under the assumption of far-field and planar wave propagation, the complex CIR between the $n$th element of the Rx

978-1-4244-1722-3/08/$25.00 ©2008 IEEE.

array and the $m$th element of the Tx array is modeled as

$$h_{n,m}(t;\tau) \doteq \sum_{\ell=1}^{L} \alpha_\ell \exp\{j2\pi f_{d\ell} t\} \\ c_{1,m}(\Omega_{1,\ell}) c_{2,n}(\Omega_{2,\ell}) \delta_m(t-\tau_\ell), \quad (2)$$

where the parameters $\{\Omega_{1,\ell}, \Omega_{2,\ell}, \alpha_\ell, \tau_\ell, f_{d\ell}\}$ of the $\ell$th wave denote, respectively, direction of departure, direction of arrival, complex weight, propagation delay, and Doppler shift. $L$ is the total number of paths. The antenna response of the $m$th element in Tx array is given by

$$c_{1,m}(\Omega_{1,\ell}) = g_{1,m}(\Omega_{1,\ell}) \exp\{j2\pi\lambda^{-1}(\Omega_{1,\ell} \cdot r_{1,m})\}, \quad (3)$$

where $g_{1,m}(\Omega_{1,\ell})$ is the complex electric field pattern of the $m$th element relative to the angle of departure (AoD) $(\phi_{1,\ell}, \theta_{1,\ell})$ of the $\ell$th path, $\lambda$ is the wavelength, and $(\cdot)$ denotes the scalar product. $c_{2,n}(\Omega_{2,\ell})$ is constructed in the similar way but relative to the angle of arrival (AoA) $(\phi_{2,\ell}, \theta_{2,\ell})$.

In order to extract the multi-dimensional parameters $\{\phi_{1,\ell}, \theta_{1,\ell}, \phi_{2,\ell}, \theta_{2,\ell}, \alpha_\ell, \tau_\ell, f_{d\ell}\}, \ell = 1, \cdots, L$ from measured CIRs, a Space-Alternating Generalized Expectation-maximization (SAGE) algorithm [11] is used to extract the parameters of multipath components (MPCs) in our investigation.

## III. Channel Measurements Campaign

### A. Measurement System

Wideband channel data were collected by the MIMO channel sounder Propsound [12], which uses the pseudo random binary signals (PRBS) and the time-division multiplexed (TDM) switching. The transmitted power was 26 dBm. The length of the PRBS was 511 and 1022 for indoor and outdoor measurements, respectively. Tx was equipped with a dual-polarized omni-directional array (ODA) with maximum 50 elements. Rx employed a vertically polarized 8-element uniform circular array (UCA). Fig. 1 depicts the configurations of Tx and Rx antenna arrays. The spacing between the neighboring elements in the ODA and the UCA is half-a-wavelength. Among the measured data, one snapshot refers to the time period separating two consecutive sounding intervals where the same Tx element is active and the same Rx element is scanned.

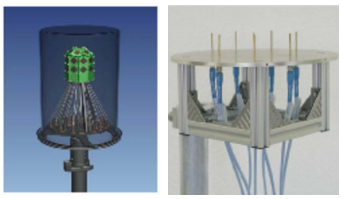

(a) (b)

Fig. 1. Configurations of the antenna arrays used in the measurements. (a) Tx array. (b) Rx array.

### B. Measurement Environments

Indoor stationary measurements were performed in the corridor of a teach building. The dimension of a single floor is 120 m $\times$ 45 m $\times$ 6 m. Tx array and Rx array were located about 1.5 m and 2.5 m above the floor level, respectively. In this scenario, the number of antenna elements of MIMO channel is $M = 50$ and $N = 8$. Fig. 2(a) illustrates the layout of indoor measurements in the corridor. Rx was fixed as the base station and marked with the arrow denoting the reference direction. For the line-of-sight (LOS) measurements, Tx was measured following 32 dots marked in the area 'Tx Grid'. At each spot, 100 snapshots of raw data were recorded. In this environment, the walls along the corridor and between the rooms are made of bricks with plasterboard on the surface. The floor is covered with marble. The doors of the rooms are wooden. The entrance doors are made of glass with aluminum frames.

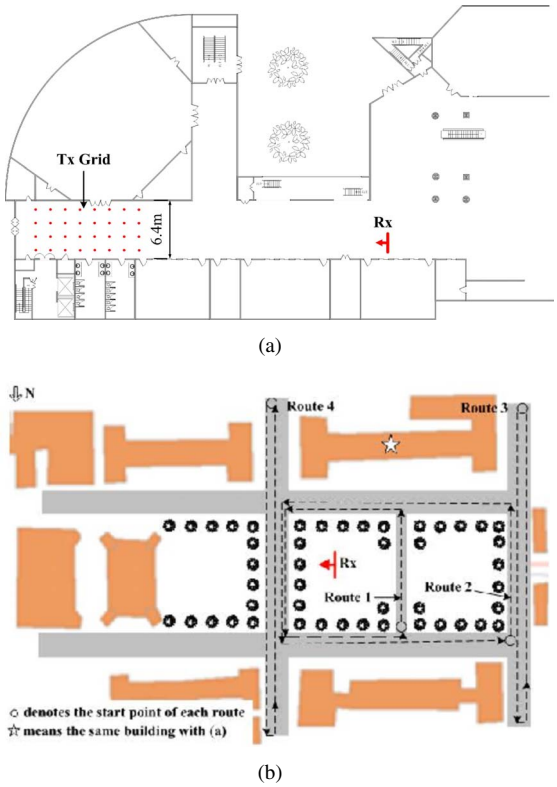


Fig. 2. Measurement scenarios. (a) Top view of indoor measurements. (b) Measured routes in the outdoor scenario.

In the outdoor hotspot scenario, mobile measurements were conducted following four routes along the streets. These routes are marked as the dashed lines in Fig. 2(b). The lengths of these routes were from 380 m to 520 m. Rx was fixed with antenna height of about 3 m as the base station and marked with the arrow denoting the reference direction. Tx was mounted on the top of a car with the average speed of nearly 15 km/h and antenna height of 2 m. The number of elements in antenna array is $M = 18$ and $N = 8$. The recorded channel data were about 1500 snapshots for each route. The

streets were bordered by trees, and Rx was surrounded by trees, grasses, two sculptures, lamp poles, etc. The propagation in this scenario can be characterized as LOS/obstructed-line-of-sight (OLOS).

Compared with system parameters of indoor scenario, the increased PRBS length and reduced number of Tx antenna elements are determined by considering the fact that, in the outdoor scenario the maximum excess delay of MPCs is larger than indoor environment and coherent time decreases due to the terminal mobility.

## IV. Measured Results and Discussion

The collected CIR data are in the form of $\mathbf{H}_{N\times M\times K\times I}$, where $K$ denotes the length of PRBS, and $I$ denotes the number of snapshots. During the indoor and outdoor measurements, the number of elements in Rx array is always $N = 8$, and $M > N$. In the initialization of SAGE, $L$ is large enough so as to capture all the possible paths, i.e., $L = 50$ in the indoor scenario, $L = 30$ in the outdoor scenario. The resolution of delay and angle estimation is 0.5 ns and $0.1^\circ$.

For the wideband MIMO system, we process the eigenvalues in different way from [8, Eq. (2)]. First, in order to separate the actual MPCs from noise, the dynamic noise floor $P_{noise}$ is calculated for each snapshot. $P_{peak}$ denotes the peak of the power delay profile (PDP). The dynamic range $D_r$ in indoor LOS scenario is 25 dB, and $D_r$ in outdoor LOS/OLOS scenario is 18 dB. The margin $D_m$ is 6 dB. Through the validation by measured data, the delay search threshold $P_{th}$ is proposed as follows

$$P_{th} = \max\{P_{noise} + D_m, P_{peak} - D_r\}. \tag{4}$$

Then the paths with power $|\mathbf{H}(t,\tau)|^2$ lower than $P_{th}$ are discarded. The remains are regarded as the actual MPCs. Using the Fourier transform, we can get the transfer function $\mathbf{H}(t,f)$. As the measured data are discrete, $\mathbf{H}(t,f)$ reduces to $\mathbf{H}_i(f_k), i = 1,\cdots,I; k = 1,\cdots,K$.

### A. Frequency-dependent eigenvalues

Using the eigenvalue decomposition (EVD), the frequency dependent covariance matrix of the $i$th snapshot is given by

$$\mathbf{R}_i(f_k) = \mathbf{H}_i(f_k)\mathbf{H}_i^\dagger(f_k) = \sum_{n=1}^{N} \lambda_{i,n}(f_k)u_{i,n}(f_k)u_{i,n}(f_k)^\dagger, \tag{5}$$

where the ordered eigenvalues $\lambda_{i,1}(f_k) \geq \lambda_{i,2}(f_k) \geq \cdots \geq \lambda_{i,N}(f_k)$ represent the mean gains of $N$ parallel subchannels in spatial domain at the $k$th frequency subchannel, $u_{i,n}(f_k)$ is the eigenvector of the $n$th eigenvalue. A normalization for the $k$th frequency subchannel of the $i$th snapshot

$$||\mathbf{H}_i(f_k)||_F^2 = NM \tag{6}$$

is applied. Here $||\cdot||_F$ denotes the Frobenius norm. For comparative purpose, all the eigenvalues are weighted by $\frac{1}{M}$ in indoor and outdoor scenarios. Thus, the upper limit of the eigenvalues is $N$.

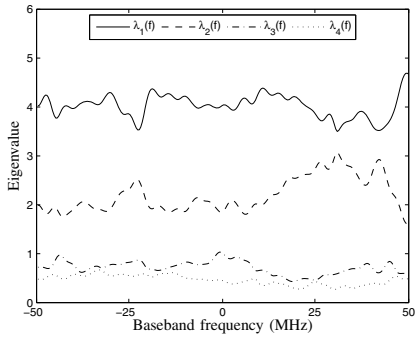


(a)

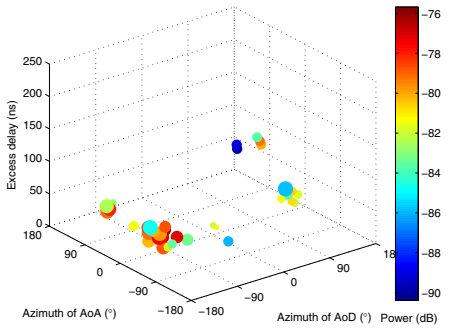


(b)

Fig. 3. Measured results of one snapshot in indoor LOS scenario. (a) Frequency-dependent eigenvalues. (b) Estimated MPCs. The size of the ball is proportional to the elevation of AoD.

Fig. 3 and Fig. 4 illustrate the four largest eigenvalues $\lambda_1(f),\cdots,\lambda_4(f)$ and the associated MPCs estimated by SAGE of one snapshot in two scenarios. It's observed that the frequency selectivity in Fig. 4(a) is much more significant than Fig. 3(a), which corresponds to the degree of delay dispersion. The root mean square (rms) delay spread shown in Fig. 3(b) and Fig. 4(b) is 20.9 ns and 30.1 ns, respectively. The empirical results of delay spread are presented in [13]. Viewed at the $k$th frequency subchannel, it appears in Fig. 4(b) that only $\lambda_1(f)$ is the dominant eigenvalue, while other eigenvalues are much close. In Fig. 4(a), $\lambda_1(f)$, $\lambda_2(f)$ and $\lambda_3(f)$ are spaced clearly over the whole bandwidth. This can be numerically evaluated by the condition number as follows.

### B. Statistics of $\lambda_{max}$ and $\lambda_{min}$

The largest eigenvalue $\lambda_{max}$ is a good predictor for diversity gain and beamforming gain [3], [14]. The smallest eigenvalue $\lambda_{min}$ impacts the multiplexing gain since it is linked to the minimum distance between received signal vectors [15]. For ease of analysis about the individual eigenvalue in spatial domain, we average over the frequency domain, expressed as

$$\bar{\lambda}_n(i) = \frac{1}{B}\int_B \lambda_{i,n}(f)df. \tag{7}$$

Let $\lambda_{max}(i) = \bar{\lambda}_1(i)$, $\lambda_{min}(i) = \bar{\lambda}_N(i)$. Then the average eigenvalue statistics $\lambda_{max}$ and $\lambda_{min}$ are tested to find out the

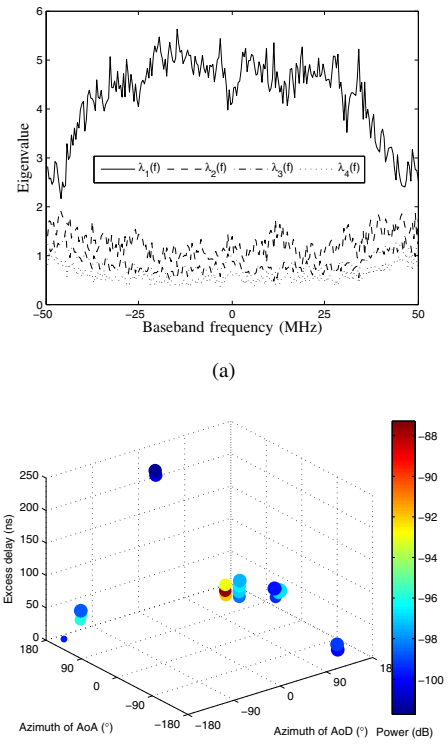


(a)

(b)

Fig. 4. Measured results of one snapshot in outdoor LOS/OLOS scenario. (a) Frequency-dependent eigenvalues. (b) Estimated MPCs. The size of the ball is proportional to the elevation of AoD.

best fit.

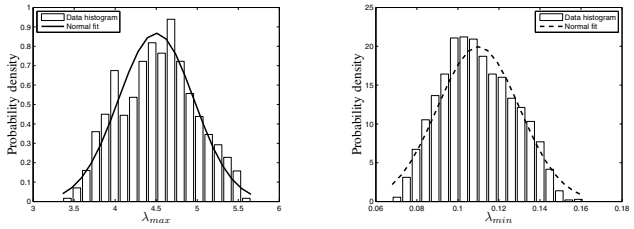


(a) (b)

Fig. 5. Empirical pdfs and fitted normal distribution of eigenvalues in indoor LOS scenario. (a) $\lambda_{max}$. (b) $\lambda_{min}$.

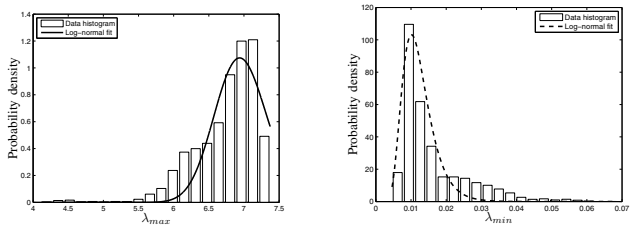


(a) (b)

Fig. 6. Empirical pdfs and fitted log-normal distribution of eigenvalues in outdoor LOS/OLOS scenario. (a) $\lambda_{max}$. (b) $\lambda_{min}$.

The goodness of fit is verified using the measure of the minimum mean square error. In indoor LOS scenario, the normal distribution

$$p(\lambda) = \frac{1}{\sqrt{2\pi}\sigma} \exp\{-\frac{(\lambda-\mu)^2}{2\sigma^2}\}, \lambda > 0 \tag{8}$$

is well fitted to model both $\lambda_{max}$ and $\lambda_{min}$. The measured pdfs are shown in Fig. 5 together with the fitted curves. In outdoor LOS/OLOS scenario, Fig. 6 illustrates that the measured pdf are unsymmetrical, and the log-normal distribution is proposed to fit the distribution:

$$p(\lambda) = \frac{1}{\sqrt{2\pi}\sigma\lambda} \exp\{-\frac{(\ln(\lambda)-\mu)^2}{2\sigma^2}\}. \tag{9}$$

The fitted parameters are listed in Table I.

TABLE I
FITTED PARAMETERS OF $\lambda_{max}$ AND $\lambda_{min}$.

| Scenarios | Eigenvalue | $\mu$ | $\sigma$ |
|---|---|---|---|
| indoor | $\lambda_{max}$ | 0.45 | 0.46 |
| LOS | $\lambda_{min}$ | 0.11 | 0.02 |
| outdoor | $\lambda_{max}$ | 1.94 | 0.05 |
| LOS/OLOS | $\lambda_{min}$ | -4.46 | 0.35 |

### C. Statistics of condition number

As the spatial selectivity indicator of the double-directional MIMO channel, the condition number of correlation matrix is evaluated, given by

$$D_\lambda(i) = \frac{\lambda_{max}(i)}{\lambda_{min}(i)}, 1 \le D_\lambda \le \infty. \tag{10}$$

The empirical cumulative distribution functions (cdfs) of $D_\lambda$ in Fig. 7 show that in outdoor LOS/OLOS scenario, the spatial correlation across the array elements is much higher than that in indoor scenario. This indicates that it is more suitable to employ the spatial multiplexing technique in indoor LOS scenario. Although the LOS path exists, the multipath effect is still significant due to the reflections and scattering of the ceiling, floor, walls and other objects involved in the environment. This observation is consistent with the average envelope correlation curves over arbitrary antenna spacing in [13].

### D. 3D Directional Spread

For the considered indoor and outdoor environments, both Tx and Rx are within the 3D scattering mechanism. The root second central moment of the direction of MPCs can characterize the mount of spatial dispersion for MIMO systems. Using the direction $\Omega$ defined in (1) and estimated parameters in (2) using SAGE, the 3D directional spread [16] is calculated as

$$\sigma_\Omega = \sqrt{\frac{\sum_{\ell=1}^{L} |\alpha_\ell|^2 |\Omega_\ell - \mu_\Omega|^2}{\sum_{\ell=1}^{L} |\alpha_\ell|^2}}, \tag{11}$$

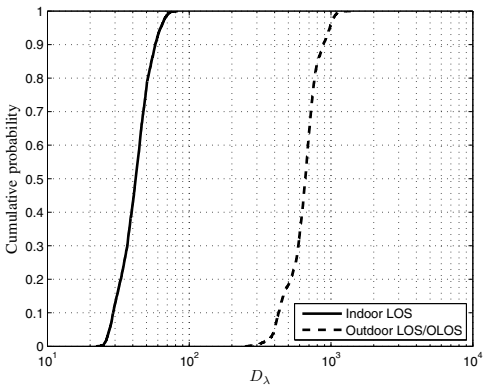


Fig. 7. Empirical cdfs of $D_\lambda$.

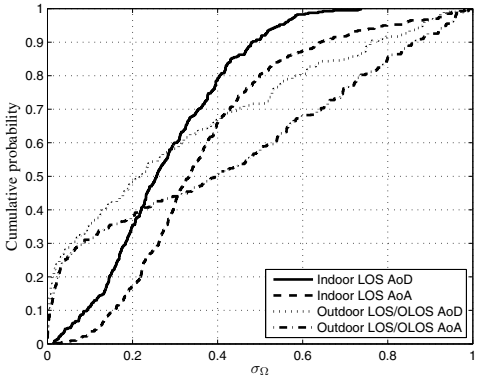


Fig. 8. Empirical cdfs of 3D directional spread in indoor and outdoor scenarios.

where $\mu_\Omega$ is the mean direction, given by

$$\mu_\Omega = \frac{\sum_{\ell=1}^{L} |\alpha_\ell|^2 \Omega_\ell}{\sum_{\ell=1}^{L} |\alpha_\ell|^2}. \quad (12)$$

Since $\Omega$ has unit norm, $|\mu_\Omega| \leq 1$, and $\sigma_\Omega^2 = 1 - |\mu_\Omega|^2$, $0 \leq \sigma_\Omega \leq 1$. The cdfs of the directional spread are plotted in Fig. 8. We separate the AoA and AoD because only directions are considered here, however this independence does not generally hold for MIMO coefficients [17]. There are cross points between the curves of AoD at 58 % and AoA at 44 %. At 50 %, the 3D directional spread is derived as 0.26, 0.33, 0.22 and 0.39 for indoor AoD, AoA, and outdoor AoD, AoA respectively.

## V. Conclusions

In this paper, the eigenvalue statistics and spatial characteristics are investigated using the measured wideband MIMO channel data. The frequency-dependent eigenvalues are the important information for the design of MIMO-OFDM technique. After averaging over all the frequency subchannels, the empirical pdfs of $\lambda_{max}$ and $\lambda_{min}$ are well fitted using the normal distribution in indoor scenario, and the log-normal distribution in outdoor scenario. These two statistics are important to evaluate the beamforming/diversity gain, and multiplexing gain in MIMO systems. The empirical cdfs of condition number and 3D directional spread are presented. Comparative analysis over two scenarios implies that spatial selectivity is much higher in indoor LOS scenario, and feasible to exploit the multiplexing gain, although no large difference is found only in terms of the 3D directional spread of AoA and AoD.

## References


[1] C. Brunner, W. Utschick, and J. A. Nossek, "Exploiting the short-term and long-term channel properties in space and time: eigenbeamforming concepts for the BS in WCDMA," *European Transactions on Telecommunications, Special Issue on Smart Antennas*, vol. 12, no. 5, pp. 365–378, 2001.

[2] R. W. Heath and A. Paulraj, "Characterization of MIMO channels for spatial multiplexing systems," in *Proc. IEEE Int. Conf. Commun.*, vol. 2, June 2001, pp. 591–595.

[3] S. A. Bjerke and I. G. Proakis, "Multiple-antenna diversity techniques for transmission over fading channels," in *Proc. IEEE Wireless Commun. and Networking Conf.*, Sep. 1999, pp. 1038–1042.

[4] T. W. Anderson, *An Introduction to Multivariate Statistical Analysis*, 2nd ed. New York: Wiley, 1984.

[5] A. Edelman, "Eigenvalues and condition numbers of random matrices," Ph.D. dissertation, Massachusetts Inst. Technol., Cambridge, MA, 1989.

[6] R. R. Muller, "On the asymptotic eigenvalue distribution of concatenated vector-valued fading channels," *IEEE Trans. Inform. Theory*, vol. 48, no. 7, pp. 2086–2091, July 2002.

[7] C. Martin and B. Ottersten, "Asymptotic eigenvalue distributions and capacity for MIMO channels under correlated fading," *IEEE Trans. Wireless Commun.*, vol. 3, no. 4, pp. 1350–1359, July 2004.

[8] H. Hofstetter, I. Viering, and W. Utschick, "Evaluation of suburban measurements by eigenvalue statistics," *in Proc. 1st COST 273 Workshop and 4th Management Committee Meeting*, May 2002.

[9] A. Taparugssanagorn, T. Jasma, and J. Ylitalo, "Spatial correlation and eigenvalue statistics investigation of wideband MIMO channel measurements," in *Proc. IEEE Int. Symposium Personal, Indoor and Mobile Radio Commun.*, 2006, pp. 1–5.

[10] X. Yin, B. H. Fleury, P. Jourdan, and A. Stucki, "Polarization estimation of individual propagation paths using the SAGE algorithm," in *Proc. IEEE Int. Symposium Personal, Indoor and Mobile Radio Commun.*, vol. 2, Sep. 2003, pp. 1795–1799.

[11] B. H. Fleury, M. Tschudin, R. Heddergott, D. Dahlhaus, and K. L. Pedersen, "Channel parameter estimation in mobile radio environments using the SAGE algorithm," *IEEE J. Select. Areas Commun.*, vol. 17, no. 3, pp. 434–450, Mar. 1999.

[12] A. Stucki *et. al.*, "PropSound System Specifications Document: Concept and Specifications," http://www.propsound.com/, Tech. Rep., 2001.

[13] J. Zhang, X. Gao, P. Zhang, and X. Yin, "Propagation characteristics of wideband MIMO channel in hotspot areas at 5.25 GHz," in *Proc. IEEE Int. Symposium Personal, Indoor and Mobile Radio Commun.*, Sep. 2007, pp. 1–5.

[14] A. Forenza, M. R. McKay, A. Pandharipande, R. W. Heath, and I. B. Collings, "Adaptive MIMO transmission for exploiting the capacity of spatially correlated channels," *IEEE Trans. Veh. Technol.*, vol. 56, no. 2, pp. 619–630, Mar. 2007.

[15] G. Burel, "Statistical analysis of the smallest singular value in MIMO transmission systems," in *Proc. WSEAS Int. Conf. Signal, Speech, Image. Process.*, vol. 447, Sep. 2002, pp. 154–158.

[16] B. H. Fleury, "First- and second-order characterization of direction dispersion and space selectivity in the radio channel," *IEEE Trans. Inform. Theory*, vol. 46, no. 6, pp. 2027–2044, Sep. 2000.

[17] H. Ozcelik, M. Herdin, W. Weichselberger, J. Wallace, and E. Bonek, "Deficiencies of "kronecker" MIMO radio channel model," *Electronics Letters*, vol. 39, no. 16, pp. 1209–1210, 2003.